ECS Journal of Solid State Science and Technology, **8** (6) P351-P356 (2019)
2162-8769/2019/8(6)/P351/6/$38.00 © The Electrochemical Society

Band Alignment of Atomic Layer Deposited SiO_2 and Al_2O_3 on $(Al_xGa_{1-x})_2O_3$ for x = 0.2-0.65

Chaker Fares,[1,*] Max Kneiß,[2] Holger von Wenckstern,[2] Marko Tadjer,[3] Fan Ren,[1,] Eric Lambers,[4] Marius Grundmann,[2] and S. J. Pearton[5,**,z]**

[1]*Department of Chemical Engineering, University of Florida, Gainesville, Florida 32611, USA*
[2]*Universität Leipzig, Felix-Bloch-Institut für Festkörperphysik, 04103 Leipzig, Germany*
[3]*U.S. Naval Research Laboratory, Washington, DC 20375, USA*
[4]*Nanoscale Research Facility, University of Florida, Gainesville, Florida 32611, USA*
[5]*Department of Materials Science and Engineering, University of Florida, Gainesville, Florida 32611, USA*

$(Al_xGa_{1-x})_2O_3$ is attracting attention for use in heterostructure devices grown on Ga_2O_3 substrates. The band alignments of amorphous, atomic layer deposited Al_2O_3 and SiO_2 on $(Al_xGa_{1-x})_2O_3$ for x = 0.2-0.65 have been determined using high resolution X-ray photoelectron spectroscopy. The $(Al_xGa_{1-x})_2O_3$ was grown by continuous composition spread Pulsed Laser Deposition (CCS-PLD). The band alignments are type I (nested gap) in all cases, with conduction band offsets ranging from 1.57-0.67 eV for Al_2O_3 on $(Al_{0.2}Ga_{0.8})_2O_3$ to $(Al_{0.65}Ga_{0.35})_2O_3$ and 2.35-1.40 eV for SiO_2 on these same compositions. Correspondingly, the valence band offsets are all >1.25 eV for SiO_2 and 0.23-0.33eV for Al_2O_3 over this composition range. While these are the first reports for Al_2O_3 on $(Al_xGa_{1-x})_2O_3$ over such a wide composition range, our results differ by up to 0.4 eV in conduction band offsets from past studies of SiO_2 on $(Al_xGa_{1-x})_2O_3$ of a more limited composition range, which themselves have shown variations of up to 0.5eV for conduction band offsets on nominally the same composition. These differences emphasize the influence of experimental conditions in determining band alignments.
 [DOI: 10.1149/2.0261906jss]

Manuscript submitted May 13, 2019; revised manuscript received June 11, 2019. Published June 20, 2019.

The maximum solubility of Al in β-Ga_2O_3 is generally reported to be in the range 67–78%.[1–5] When grown by a variety of methods, including pulsed laser deposition and molecular beam epitaxy.[6–14] Methods for calculating the strain in pseudomorphic $(Al_xGa_{1-x})_2O_3$ heterostructures on bulk β-Ga_2O_3 substrates are also available.[11,12] There have been recent demonstrations of high quality $(Al_xGa_{1-x})_2O_3/Ga_2O_3$ heterostructures for field effect transistors with enhanced electron mobility due to formation of two-dimensional electron gases (2DEG) at the heterointerface.[14–21] For example, Zhang et al.[21] reported formation of a 2DEG in a modulation-doped β-$(Al_xGa_{1-x})_2O_3/Ga_2O_3$ structure from Hall measurements, with channel mobility of 143 $cm^2/V{\cdot}s$ at 300K and 1520 $cm^2/V{\cdot}s$ at 50 K. Such devices, if optimized, might be useful for RF power device applications. The $(Al_xGa_{1-x})_2O_3$ can also be used in solar-blind UV photodetectors.[22,23]

A key requirement in MOS-gate wide bandgap power devices is that the gate dielectric have sufficient band offsets to ensure good carrier confinement at the heterointerface with the semiconductor. A schematic of a prototypical device embodiment is shown in Figure 1, where the dielectric is used to form a MOS gate on the $(Al_xGa_{1-x})_2O_3$. The dielectric needs to be thermodynamically stable on the $(Al_xGa_{1-x})_2O_3$ and have sufficient band offsets to produce good carrier confinement. There are only a few reports of band alignments for dielectrics on $(Al_xGa_{1-x})_2O_3$ at a limited range of Al contents[24,25] or even just a single Al concentration (0.14, typical of heterostructure transistor structures).[26–29] Feng et al.[24] determined the band alignment for atomic layer deposited (ALD) SiO_2 on $(Al_xGa_{1-x})_2O_3$ with x = 0-0.49. The valence band offsets were in the range 1.5-0.8 eV for this composition range. They also reported band offsets for ALD deposited SiO_2 and HfO_2 on $(Al_xGa_{1-x})_2O_3$ with x = 0-0.53.[25] Even within these studies from the same group, differences of up to 0.5 eV in conduction band offset and 0.3 eV in valence band offset were found for SiO_2 on nominally similar Al contents in the $(Al_xGa_{1-x})_2O_3$. Such differences are not uncommon in the literature on band offsets on semiconductors and have been ascribed to the effects of dielectric deposition method on surface stoichiometry and defect density, bandgap of the dielectric, and contamination.[30] It is clearly of value to examine the band alignments over a wider range of Al contents, to measure this for Al_2O_3 because of its compatibility with $(Al_xGa_{1-x})_2O_3$ and also to measure the phase purity of the $(Al_xGa_{1-x})_2O_3$ used in the experiments.

In this paper, we utilize X-Ray Photoelectron Spectroscopy (XPS) to determine the valence band offsets in SiO_2 and $Al_2O_3/(Al_xGa_{1-x})_2O_3$ heterostructures with x = 0.2−0.65, in which amorphous dielectrics were deposited by ALD onto $(Al_xGa_{1-x})_2O_3$ grown by continuous composition spread Pulsed Laser Deposition (CCS-PLD).[1,13] In these films, the monoclinic phase is phase pure up to ∼40-45 at.%, then a mixed phase with γ-$(Al_xGa_{1-x})_2O_3$ is present. Above roughly 50–55 at.%, the thin film shows purely the γ-phase. SiO_2 is found to have both conduction band and valence band offsets >1.2 eV over the entire composition range examined, while Al_2O_3 has relatively small valence band offsets (eV) over this composition range.

Experimental

The $(Al_xGa_{1-x})_2O_3$ films with x = 0.15-0.70 were grown on (100) MgO substrates by continuous composition spread Pulsed Laser Deposition (CCS-PLD), which relies on the ablation of segmented PLD targets.[13,31] This CCS-PLD method can be used in existing off-set PLD systems without any modification of the hardware. A spatial offset between the substrate center and the centerline of the expanding plasma plume and a synchronized rotation of substrate and semicircular-segmented targets (lateral target segmentation) are used to obtain a lateral continuous composition spread.[1,13] The distribution of the different elements originating from different target segments on the substrate depends on background pressure, target-to-substrate distance, and the offset, as well as the normal thermodynamic conditions for deposition.[31]

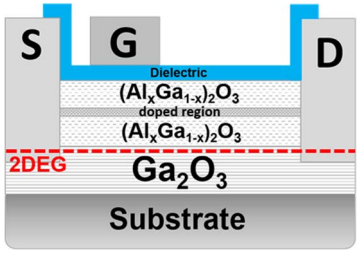

Figure 1. Typical $(Al_xGa_{1-x})_2O_3/Ga_2O_3$ HFET where gate insulator selection is crucial.

*Electrochemical Society Student Member.
**Electrochemical Society Fellow.
zE-mail: spear@mse.ufl.edu

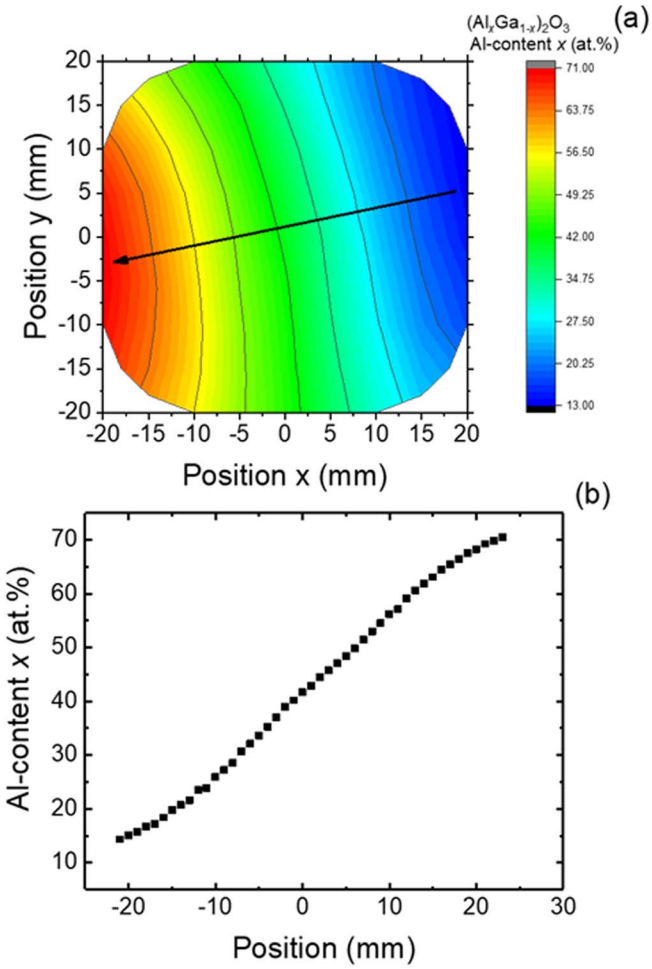

Figure 2. (a) False-color representation of the Al concentration within a two inch in diameter $(Al_{1-x}Ga_x)_2O_3$ thin film grown with continuously varying composition on (100)MgO. (b) Line scan of Al content as a function of position along the wafer determined by EDX along the gradient direction depicted as black arrow in (a).

The lateral variation of the Al content of a $(Al_xGa_{1-x})_2O_3$ thin film grown by CCS-PLD using a target consisting of semicircular Al_2O_3 and Ga_2O_3 segments is shown in Figure 2a. Energy-dispersive X-ray spectroscopy (EDX) was used for the spatially resolved chemical analysis, where a Nova Nanolab 200 system by FEI company was employed. The sample was deposited at a growth temperature of 650°C and an oxygen pressure 0.08 mbar on a two inch in diameter (100) MgO substrate. The Al concentration varies between 0.15 and 0.70, as shown in Figure 2b and has a slight S-shaped dependence along the gradient direction, in agreement with calculations.[13] Along lines perpendicular to the gradient direction the Al concentration is in principle constant. Figure 3 shows a false color representation of X-ray diffractograms along the compositional gradient. As discussed above, there is pure monoclinic phase up to ~40-45 at.%, then a mixed phase with γ-$(Al_xGa_{1-x})_2O_3$ is present. Above ~50-55 at.%, the films show pure γ-phase. More details of the growth are given elsewhere.[6,13]

The ALD layers were deposited at 200°C in remote plasma mode in a Cambridge Nano Fiji 200 using a trimethylaluminum precursor or Tris (dimethylamino) silane and an inductively coupled plasma (ICP) at 300 W to generate atomic oxygen.[26–29] For substrate cleaning prior to deposition, a rinse sequence consisting of acetone and IPA was followed by drying in filtered N_2, and finally ozone exposure for 15 min. After this substrate cleaning, samples were directly loaded into the deposition systems within a cleanroom environment to avoid contamination of the deposited films. Both thick (200 nm) and thin

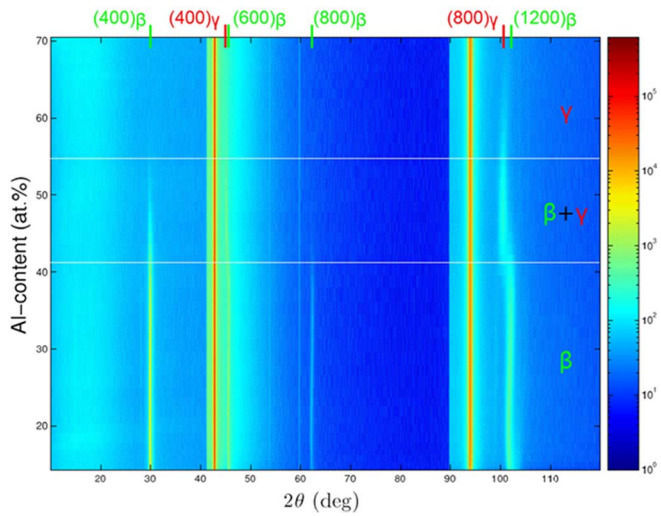

Figure 3. False-color representation of θ-2θ X-ray diffractograms acquired along the compositional gradient of a $(Al_xGa_{1-x})_2O_3$ CCS-PLD sample deposited on (100) MgO substrates deposited at about 650°C.

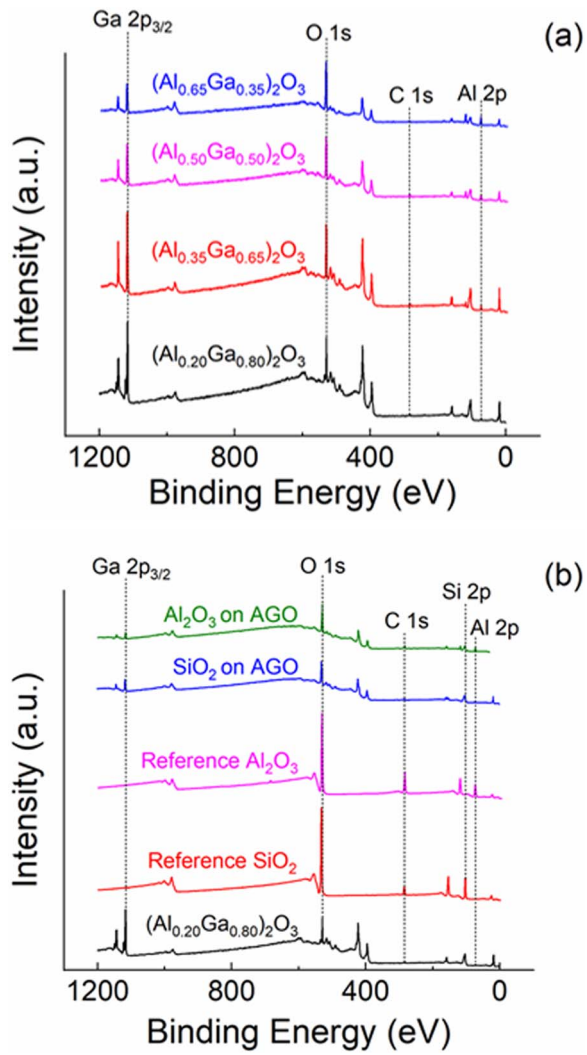

Figure 4. XPS survey scans of (a) $(Al_xGa_{1-x})_2O_3$ at the aluminum concentrations studied in this report and (b) thick ALD Al_2O_3, thick ALD SiO_2, and heterostructures of each oxide on AGO. The intensity is in arbitrary units (a.u.).

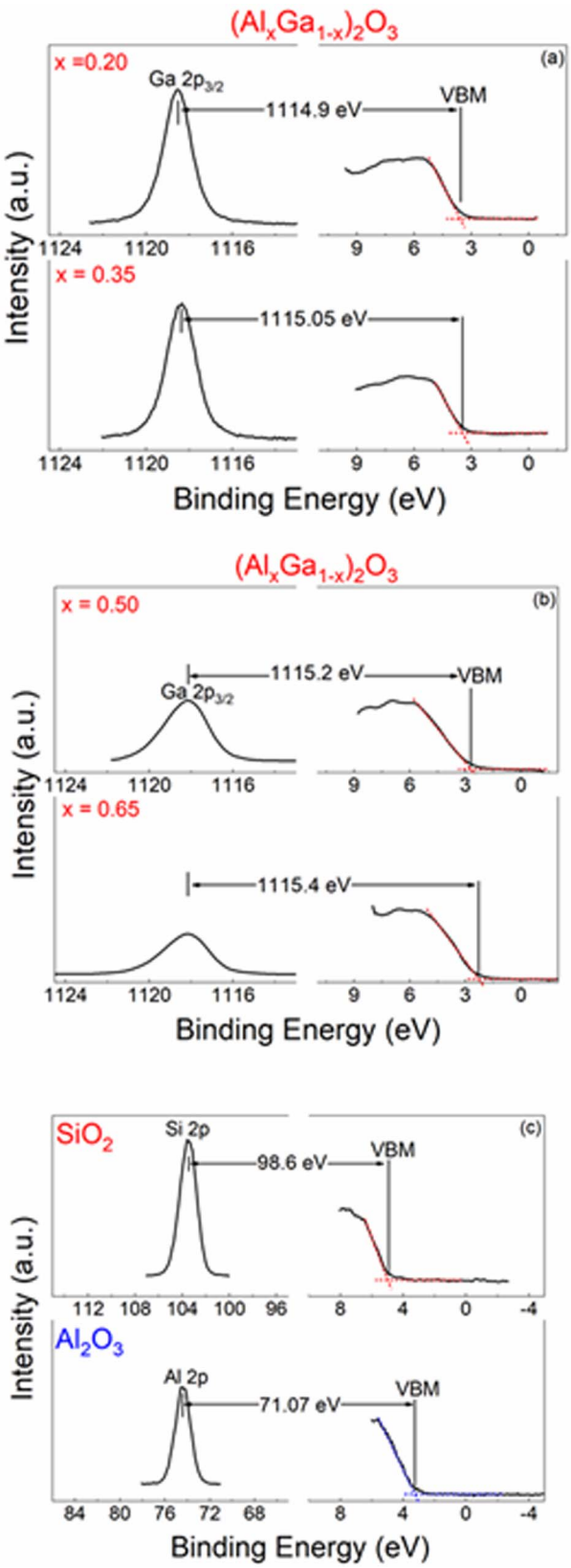

Figure 5. XPS spectra of core levels to valence band maximum (VBM) for (a) reference $(Al_xGa_{1-x})_2O_3$ with 20% and 35% Aluminum, (b) reference $(Al_xGa_{1-x})_2O_3$ with 50% and 65% Aluminum, and (c) ALD thick film Al_2O_3 and SiO_2. The intensity is in arbitrary units (a.u.).

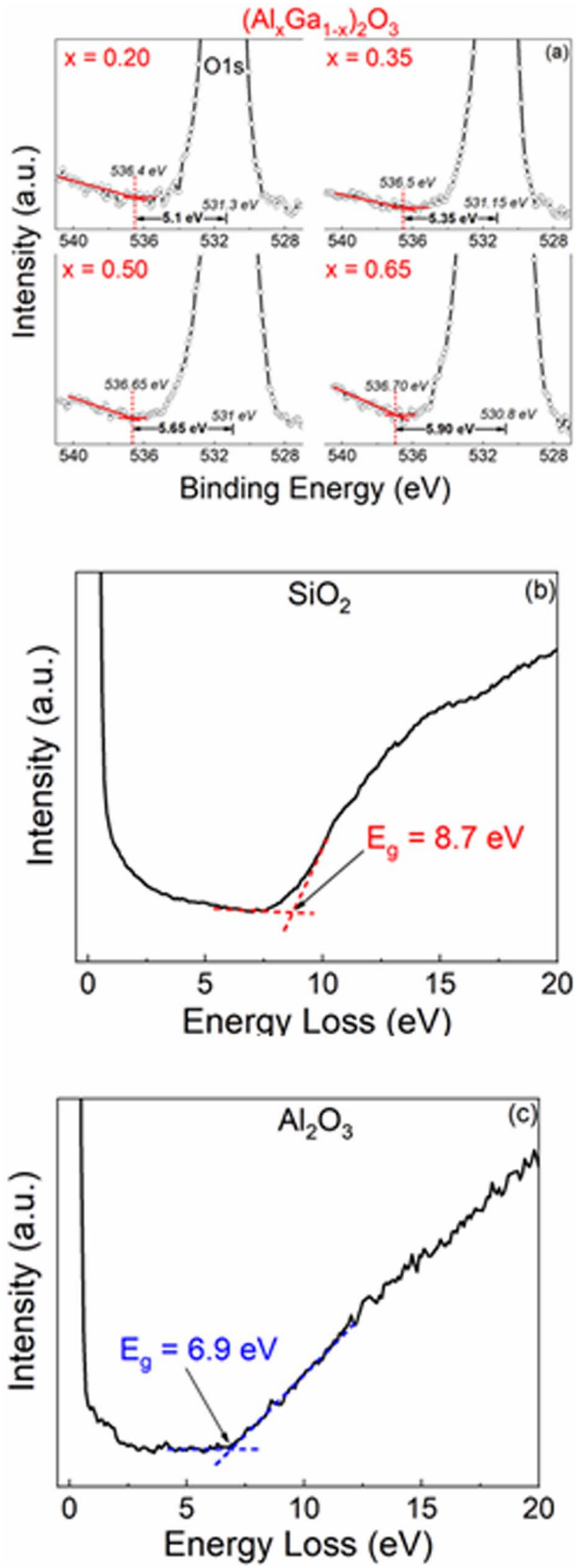

Figure 6. Bandgap of (a) $(Al_xGa_{1-x})_2O_3$ determined using the onset of the plasmon loss feature in O 1s photoemission spectrum, (b) ALD SiO_2, and (c) ALD Al_2O_3 where both deposited films' bandgap was determined by Reflection Electron Energy Loss Spectra. The intensities are in arbitrary units (a.u.).

Table I. Summary of the measured reference and heterostructure peaks for SiO_2 on $(Al_xGa_{1-x})_2O_3$ (eV).

Aluminum Concentration	Reference $(Al_xGa_{1-x})_2O_3$ Core Level Peak (Ga $2p_{3/2}$)	VBM	Core - VBM	Reference SiO_2 Core Level Peak (Si 2p)	VBM	Core - VBM	Thin SiO_2 on $(Al_xGa_{1-x})_2O_3$ Δ Core Level (Ga $2p_{3/2}$ - Si 2p)	Valence Band Offset
$(Al_{0.20}Ga_{0.80})_2O_3$	1118.50	3.6	1114.90	103.40	4.80	98.60	1115.05	1.25
$(Al_{0.35}Ga_{0.65})_2O_3$	1118.35	3.3	1115.05	-	-	-	1115.10	1.3
$(Al_{0.50}Ga_{0.50})_2O_3$	1118.10	2.9	1115.20	-	-	-	1115.25	1.35
$(Al_{0.65}Ga_{0.35})_2O_3$	1118.00	2.6	1115.40	-	-	-	1015.40	1.4

(1.5 nm) layers of the dielectrics were deposited for measuring both bandgaps and core levels on the β-$(Al_xGa_{1-x})_2O_3$.[30]

We used XPS survey scans to establish the chemical state of the SiO_2, Al_2O_3, and the $(Al_xGa_{1-x})_2O_3$ samples. The XPS system was a Physical Instruments ULVAC PHI, with an Al X-ray source (energy 1486.6 eV, source power 300W), analysis size of 100 μm diameter, a take-off angle of 50° and acceptance angle of ± 7 degrees. The electron pass energy was 23.5 eV for high-resolution scans and 93.5 eV for survey scans. The total energy resolution of this XPS system is about 0.5 eV, and the accuracy of the observed binding energy is within 0.03 eV.[27–30]

To avoid sample charging, charge compensation employed an electron flood gun and a simultaneous ion beam. C 1*s* core levels of the surface adsorbate (284.8 eV) were used to calibrate the binding energy. Only the relative energy position is needed to determine the valence band offsets, so the absolute energy calibration for a sample has no effect on that number.[32,33] The samples were electrically insulated from the chuck to avoid uneven charge dispersion along the sample. All electron analyzers and equipment were grounded. Differential charging was not observed in any of the samples with the use of the electron gun. The SiO_2 and Al_2O_3 bandgaps were obtained from Reflection Electron Energy Loss Spectroscopy (REELS)[32,33] using a 1 kV electron beam and hemispherical electron analyzer. The bandgaps of the $(Al_xGa_{1-x})_2O_3$ for each composition were obtained from XPS energy loss measurements of the O1S peak. This is conveniently done at the same time as the band alignment measurements.

Results and Discussion

The XPS survey scans from the different compositions of $(Al_xGa_{1-x})_2O_3$ are shown in Figure 4a. The samples show only the lattice constituents. Figure 4b shows the survey spectra for the thick (200 nm) dielectrics of ALD SiO_2 and Al_2O_3, thin (1.5 nm) SiO_2 and Al_2O_3 on β-$(Al_xGa_{1-x})_2O_3$, labelled here as AGO, and the $(Al_{0.2}Ga_{0.8})_2O_3$ sample for reference.

Figure 5 shows high resolution XPS spectra for the vacuum-core delta regions of four different $(Al_xGa_{1-x})_2O_3$ compositions, namely x = 0.2 and 0.35 in (a), x = 50 and 0.65 in (b), along with the SiO_2 and Al_2O_3 in (c). The VBMs were 3.6 ± 0.2 eV for β-$(Al_{0.2}Ga_{0.8})_2O_3$, 3.3 eV for $(Al_{0.35}Ga_{0.65})_2O_3$, 2.9 eV for $(Al_{0.5}Ga_{0.5})_2O$ and 2.6 eV for $(Al_{0.65}Ga_{0.35})_2O_3$. The valence band offsets are then obtained by measuring the shift of the core levels for the heterostructure samples with the thin dielectric on top of the different compositions of $(Al_xGa_{1-x})_2O_3$.[34] We also measured the bandgaps of the $(Al_xGa_{1-x})_2O_3$ at the compositions of interest, as shown in Figure 6a, from the separation between the core level peak energy and the onset of inelastic (plasmon) losses in each O 1s photoemission spectra.[35] The respective bandgaps were 5.1 eV for $(Al_{0.2}Ga_{0.8})_2O_3$, 5.35eV for $(Al_{0.35}Ga_{0.65})_2O_3$, 5.65 eV for $(Al_{0.5}Ga_{0.5})_2O_3$ and 5.90 eV for $(Al_{0.65}Ga_{0.35})_2O_3$. These are in excellent agreement with the relationship reported previously for the compositional dependence of bandgap (E_g) of $(Al_xGa_{1-x})_2O_3$, namely[1,7,36]

$$E_g = (4.75 + 1.87x)\,\text{eV}$$

Using this relationship, we would expect values of 5.1eV for x = 0.2, 5.4 eV for x = 0.35, 5.68 eV for x = 0.50 and 5.97 eV for x = 0.65., ie. the differences from our experimental values are <0.07 eV across the composition range studied here. Values of the indirect bandgap using the formula $E_g = 4.637 + 1.87x$, determined by Schmidt-Grund et al.[7] on a similar CCS-PLD sample by using spectroscopic ellipsometry, are 5.01 eV, 5.29 eV, 5.57 eV and 5.85 eV for x = 0.2, 0.35, 0.5 and 0.65, respectively, which is in good agreement to the values determined by XPS. Other experimental values for similar compositions reported from studies by Feng et al.[25,26] include 5.1 eV (x = 0.35), 5.3eV (x = 0.33), 5.43 eV (x = 0.30), 5.2eV (x = 0.40), 5.64 eV (x = 0.49), and 5.4 eV (x = 0.53). Obviously, within similar groups of samples in those cases, there was variation of ∼0.2 eV. Wakabayashi et al.[20] reported that strain in layers of $(Al_xGa_{1-x})_2O_3$ might lead to bowing of the bandgap with composition. Figures 6b and 6c shows the REELS spectra to determine the bandgap of the SiO_2 and Al_2O_3, respectively, with values of 8.7 eV and 6.9 eV, respectively. These are consistent with previous reported values.[26–30]

Tables I and II show the valence band maximum (VBM) for the dielectrics and the $(Al_xGa_{1-x})_2O_3$ obtained using linear fitting of the leading edge of the valence band. Figure 7 shows the core energy differences from XPS spectra for $(Al_xGa_{1-x})_2O_3$ to SiO_2 for compositions of 0.20 and 0.35 (a) and 0.50 and 0.65 (b), respectively, as well as $(Al_xGa_{1-x})_2O_3$ to Al_2O_3 for compositions of 0.20 and 0.35 (c) and 0.50 and 0.65 (d), respectively. The core energy levels and the differences between Ga 2p3/2 and Si 2p or Al 2p core energy levels, respectively, are shown in the figure. We used the usual method to measure the valence band offsets by observing the shift of the core levels from the $(Al_xGa_{1-x})_2O_3$ when SiO_2 or Al_2O_3 was deposited.[35] This method measures the energy difference between a core level and the VBM for both the single layer dielectric and $(Al_xGa_{1-x})_2O_3$. The separation between the reference core levels can be translated into the valence band offset (VBO) using the previously measured single layer sample core-level to valence band maximum (VBM) energies.[35] The VBM

Table II. Summary of the measured reference and heterostructure peaks for Al_2O_3 on $(Al_xGa_{1-x})_2O_3$ (eV).

Aluminum Concentration	Reference $(Al_xGa_{1-x})_2O_3$ Core Level Peak (Ga $2p_{3/2}$)	VBM	Core - VBM	Reference Al_2O_3 Core Level Peak (Al 2p)	VBM	Core - VBM	Thin Al_2O_3 on $(Al_xGa_{1-x})_2O_3$ Δ Core Level (Ga $2p_{3/2}$ - Al 2p)	Valence Band Offset
$(Al_{0.20}Ga_{0.80})_2O_3$	1118.50	3.6	1114.90	74.32	3.25	71.07	1043.60	0.23
$(Al_{0.35}Ga_{0.65})_2O_3$	1118.35	3.3	1115.05	-	-	-	1043.70	0.28
$(Al_{0.50}Ga_{0.50})_2O_3$	1118.10	2.9	1115.20	-	-	-	1043.80	0.33
$(Al_{0.65}Ga_{0.35})_2O_3$	1118.00	2.6	1115.40	-	-	-	1044.00	0.33

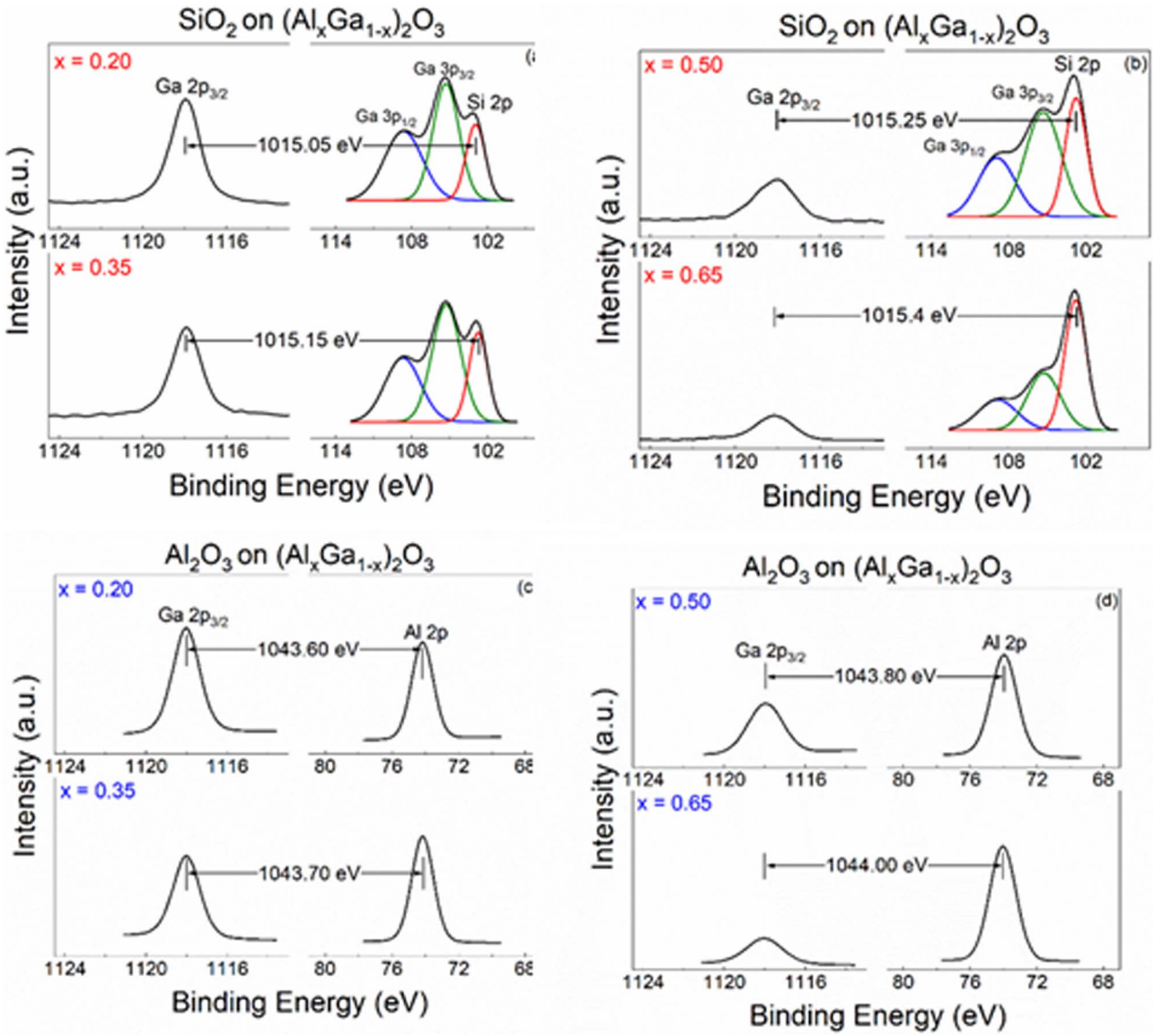

Figure 7. High resolution XPS spectra for the (a-b.) $(Al_xGa_{1-x})_2O_3$ to SiO_2 core delta regions and the (c-d.) $(Al_xGa_{1-x})_2O_3$ to Al_2O_3 core delta regions. The intensity is in arbitrary units (a.u.).

values were determined by linear extrapolation of the leading edge to the baseline of the valence band spectra. The error bars in the different binding energies were combined in a root sum square relationship to determine the overall error bars in the valence band offsets.[30]

The valence band offsets for SiO_2 were 1.25 ± 0.20 eV for β-$(Al_{0.2}Ga_{0.8})_2O_3$, 1.3 ± 0.20 eV for $(Al_{0.35}Ga_{0.65})_2O_3$, 1.35 ± 0.20 eV for $(Al_{0.5}Ga_{0.5})_2O$ and 1.4 ± 0.20 eV for $(Al_{0.65}Ga_{0.35})_2O_3$. Based on the measured bandgap of this dielectric, the conduction band offsets are then 2.35 eV (x = 0.2), 2.20 eV (x = 0.35), 1.7 eV (x = 0.4) and 1.4 eV (x = 0.65). SiO_2 therefore provides excellent confinement of electrons in $(Al_xGa_{01-x})_2O_3$ samples over the practical range of Al contents achievable. The SiO_2/β-$(Al_xGa_{1-x})_2O_3$ band alignment remained type I across the entire composition range examined here, as shown in the schematic of Figure 8. Note that our valence band offsets are 0.10-0.45 eV different (both larger or smaller, depending on composition) than reported by Feng et al.[24,25] for similar deposition conditions for the SiO_2 on $(Al_xGa_{01-x})_2O_3$ of comparable compositions to those used here. There are no obvious signs of metal contamination in the reported XPS survey spectra, so this gives an idea of the inherent accuracy of comparing valence band offsets values in the literature for the same dielectric/semiconductor systems.

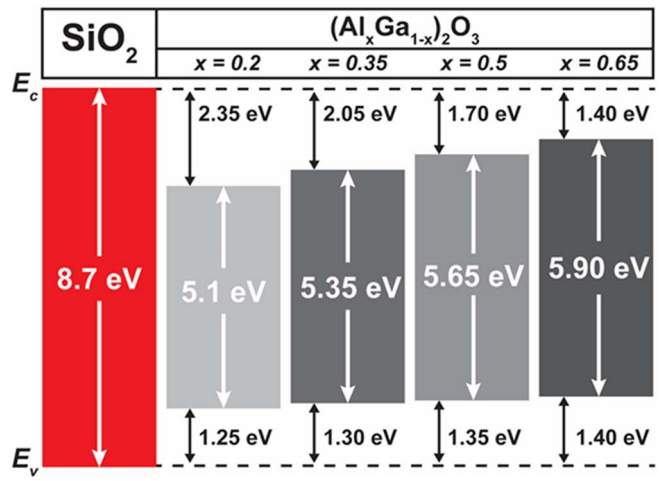

Figure 8. Band diagrams for the $SiO_2/(Al_xGa_{1-x})_2O_3$ heterostructure in which the SiO_2 was deposited by ALD.

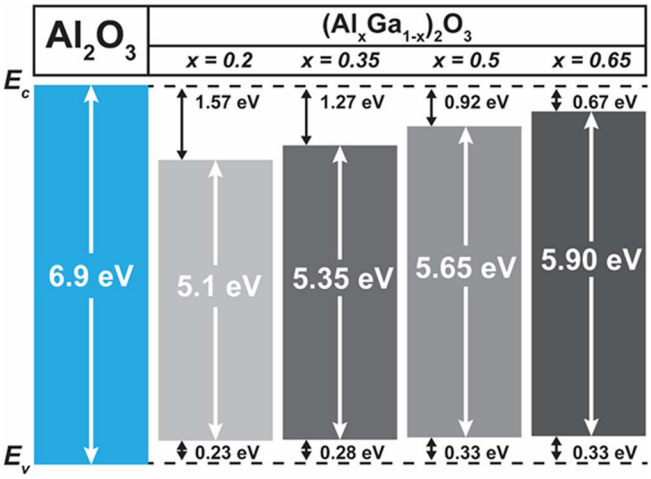

Figure 9. Band diagrams for the $Al_2O_3/(Al_xGa_{1-x})_2O_3$ heterostructure in which the Al_2O_3 was deposited by ALD.

The valence band offsets for Al_2O_3 were 0.23 ± 0.05 eV for β-$(Al_{0.2}Ga_{0.8})_2O_3$, 0.28 ± 0.05 eV for $(Al_{0.35}Ga_{0.65})_2O_3$, 0.33 ± 0.06 eV for $(Al_{0.5}Ga_{0.5})_2O$ and 0.33 ± 0.06 eV for $(Al_{0.65}Ga_{0.35})_2O_3$. Based on the measured bandgap of Al_2O_3, the conduction band offsets are then 1.57 eV (x = 0.2), 1.27 eV (x = 0.35), 0.92 eV (x = 0.4) and 0.67 eV (x = 0.65). The electron confinement would be marginal at high Al contents in $Al_2O_3/(Al_xGa_{1-x})_2O_3$. The band alignments are also type I, as shown in the schematic of Figure 9.

Conclusions

XPS was used to measure the valence band offsets of $SiO_2/(Al_xGa_{01-x})_2O_3$ and $Al_2O_3/(Al_xGa_{01-x})_2O_3$ heterojunctions over the widest range of Al contents reported to date (x = 0.2-0.65), in which the dielectrics were deposited by ALD. The band alignments are type I in all cases, with valence band offsets >1.25 eV for SiO_2 across the whole composition range of $(Al_xGa_{1-x})_2O_3$ examined. By contrast, the valence band offsets for Al_2O_3 are in the range 0.23-0.33 eV for the same range of Al contents in $(Al_xGa_{1-x})_2O_3$. The CCS-PLD technique provides an effective pathway to producing a wide range of compositions for study of band alignments.

Acknowledgments

We thank Jörg Lenzner for EDX measurements and Monika Hahn for PLD target preparation. The project or effort depicted was also sponsored by the Department of the Defense, Defense Threat Reduction Agency, HDTRA1-17-1-011, monitored by Jacob Calkins and also by NSF DMR 1856662 (Tania Paskova). Research at NRL was supported by the Office of Naval Research, partially under Award Number N00014-15-1-2392. M.K. acknowledges support by the European Social Fund within the Young Investigator Group "Oxide Heterostructures" (SAB 100310460) and the Leipzig School for Natural Sciences BuildMoNa.

ORCID

Chaker Fares https://orcid.org/0000-0001-9596-2381
Holger von Wenckstern https://orcid.org/0000-0002-3936-275X
Marko Tadjer https://orcid.org/0000-0002-2388-2937
Fan Ren https://orcid.org/0000-0001-9234-019X
Marius Grundmann https://orcid.org/0000-0001-7554-182X
S. J. Pearton https://orcid.org/0000-0001-6498-1256

References

1. Holger von Wenckstern, *Advanced Electronic Materials*, **3**, 1600350 (2017).
2. V. G. Hill, R. Roy, and E. F. Osborn, *J. Am. Ceram. Soc.*, **35**, 135(1952).
3. M. Mizuno, T. Yamada, and T. Noguchi, *Dainippon Yogyo Kyokai Zasshi*, **83**, 175 (1975).
4. A. L. Jaromin and D. D. Edwards, *J. Am. Ceram. Soc.*, **88**, 2573 (2005).
5. T. Oshima, T. Okuno, N. Arai, Y. Kobayashi, and S. Fujita, *Jpn. J. Appl. Phys.*, **48**, 070202 (2009).
6. C. Kranert, M. Jenderka, J. Lenzner, M. Lorenz, H. Von Wenckstern, R. Schmidt-Grund, and M. Grundmann, *J. Appl. Phys.*, **117**, 125703 (2015).
7. Rüdiger Schmidt-Grund, Christian Kranert, Holger von Wenckstern, V. Zviagin, Michael Lorenz, and Marius Grundmann, *J. Appl. Phys.*, **117**, 165307 (2015).
8. S. W. Kaun, F. Wu, and J. S. Speck, *J. Vac. Sci. Technol., A*, **33**, 041508 (2015).
9. Y. Oshima, E. Ahmadi, S. C. Badescu, F. Wu, and J. S. Speck, *Appl. Phys. Express*, **9**, 061102 (2016).
10. T. Oshima, Y. Kato, N. Kawano, A. Kuramata, S. Yamakoshi, S. Fujita, T. Oishi, and M. Kasu, *Appl. Phys. Express*, **10**, 035701 (2017).
11. M. Grundmann, *Phys. Status Solidi B*, **254**, 1700134 (2017).
12. M. Grundmann, *J. Appl. Phys.*, **124**, 185302 (2018).
13. Holger von Wenckstern, Zhipeng Zhang, Florian Schmidt, Jörg Lenzner, Holger Hochmuth, and Marius Grundmann, *Cryst Eng Comm*, **15**, 10020 (2013).
14. Y. Zhang, A. Neal, Zhanbo Xia, C. Joishi, J. M. Johnson, Y. Zheng, S. Bajaj, M. Brenner, D. Dorsey, K. Chabak, G. Jessen, J. Hwang, Shin Mou, J. P. Heremans, and S. Rajan, *Appl. Phys. Lett.*, **112**, 173502 (2018).
15. S. Krishnamoorthy, Z. Xia, C. Joishi, Y. Zhang, J. McGlone, J. Johnson, M. Brenner, A. R. Arehart, J. Hwang, and S. Lodha, *Appl. Phys. Lett.*, **111**, 023502 (2017).
16. E. Ahmadi, O. S. Koksaldi, X. Zheng, T. Mates, Y. Oshima, U. K. Mishra, and J. S. Speck, *Appl. Phys. Express*, **10**, 071101 (2017).
17. Takayoshi Oshima, Takeya Okuno, Naoki Arai, Yasushi Kobayash, and Shizuo Fujita, *Jpn. J. Appl. Phys.*, **48**, 070202 (2009).
18. Yuewei Zhang, Chandan Joishi, Zhanbo Xia, Mark Brenner, Saurabh Lodha, and Siddharth Rajan, *Appl. Phys. Lett.*, **112**, 233503 (2018).
19. Fabi Zhang, Katsuhiko Saito, Tooru Tanaka, Mitsuhiro Nishio, Makoto Arita, and Qixin Guo, *Appl. Phys. Lett.*, **105**, 162107 (2014).
20. Ryo Wakabayashi, Mai Hattori, Kohei Yoshimatsu, Koji Horiba, Hiroshi Kumigashira, and Akira Ohtomo, *Appl. Phys. Lett.*, **112**, 232103 (2018).
21. Y. Zhang, Z. Xia, J. Mcglone, W. Sun, C. Joishi, A. R. Arehart, S. A. Ringel, and Siddharth Rajan, *IEEE Trans Electron Dev*, **66**, 1574 (2019).
22. Q. Feng, X. Li, G. Han, L. Huang, F. Li, W. Tang, J. Zhang, and Y. Hao, *Opt. Mater. Express*, **7**, 1240 (2017).
23. F. Zhang, K. Saito, T. Tanaka, M. Nishio, M. Arita, and Q. Guo, *Appl. Phys. Lett.*, **105**, 162107 (2014).
24. Zhaoqing Feng, Qian Feng, Jincheng Zhang, Xiang Li, Fuguo Li, Lu Huang, Hong-Yan Chen, Hong-Liang Lu, and Yue Hao, *Appl. Surf. Sci.*, **434**, 440 (2018).
25. Zhaoqing Feng, Qian Feng, Jincheng Zhang, Chunfu Zhang, Hong Zhou, Xiang Li, Lu Huang, Lei Xu, Yuan Hu, Shengjie Zhao, and Yue Hao, *J. Alloys Comp*, **745**, 292 (2018).
26. C. Fares, F. Ren, E. S. Lambers, D. C. Hays, B. P. Gila, and S. J. Pearton, *J. Electron. Mater.*, **48**, 1568 (2019).
27. C. Fares, F. Ren, E. Lambers, D. C. Hays, B. P. Gila, and S. J. Pearton, *Semicond. Sci. Technol.*, **34**, 025006 (2019).
28. Chaker Fares, F. Ren, Eric Lambers, David C. Hays, B. P. Gila, and S. J. Pearton, *J. Vac. Sci. Technol. B*, **36**, 061207 (2018).
29. Chaker Fares, F. RenDavid C. Hays, B. P. Gila, and S. J. Pearton, *ECS J. Solid State Sci. Technol.*, **8**, Q3001 (2019).
30. D. C. Hays, B. P. Gila, S. J. Pearton, and F. Ren, *Appl. Phys. Rev.*, **4**, 021301 (2017).
31. M. Lorenz, H. Hochmuth, H. Hilmer, A. Lajn, D. Spemann, M. Brandt, J. Zippel, R. Schmidt-Grund, H. von Wenckstern, and M. Grundmann, *Laser Chem.*, Article ID 140976 (2010).
32. E. A. Kraut, R. W. Grant, J. R. Waldrop, and S. P. Kowalczyk., *Phys. Rev. Lett.*, **44**, 1620 (1980).
33. E. Bersch, M. Di, S. Consiglio, R. D. Clark, G. J. Leusink, and A. C. Diebold, *J. Appl. Phys.*, **107**, 043702 (2010).
34. H. C. Shin, D. Tahir, S. Seo, Y. R. Denny, S. K. Oh, H. J. Kang, S. Heo, J. G. Chung, J. C. Lee, and S. Tougaard, *Surf. Interface Anal.*, **44**, 623 (2012),
35. Chaker Fares, F. Ren, E. Lambers, D. C. Hayes, B. P. Gila, and S. J. Pearton, *ECS J.Solid State Sci. Technol.*, **7**, P519 (2018).
36. Benjamin W. Krueger, Christopher S. Dandeneau, Evan M. Nelson, Scott T. Dunham, Fumio S. Ohuchi, and Marjorie A. Olmstead, *J. Am. Ceram. Soc.*, **99**, 2467 (2016).